DFIG Control Design for Preventing SSR Mode

Deodatta Y. Shingare[1], Dr. Sunil Kumar T. K.[2]

[1]*Research Scholar, Dept. of Electrical Engineering, National Institute of Technology, Calicut, India*
[2]*Assistant Professor, Dept. of Electrical Engineering, National Institute of Technology, Calicut, India*

Abstract - *This paper presents novel approach to design the controller for Doubly-fed induction generator (DFIG) in Stator-Voltage-oriented (SVO) synchronous reference frame for preventing sub-synchronous resonance. The state-space model of DFIG including inner current closed loop dynamics with different feed-forward compensation schemes is developed. The inner current loop dynamics is usually ignored when SVO control is employed. The effect of inner current loop dynamics on the sub-synchronous resonance (SSR) mode of the system is illustrated through analysis and simulation. The analysis makes it clear that the stability of DFIG and also the SSR mode excitation in SVO depends mainly on the tuning of the proportional-integral (PI) controllers. Erroneous tuning results into instability and also excitation of SSR mode. This paper contributes the tuning methodology of the PI-controllers in order to secure the stability of DFIG and also the additional advantage of preventing SSR mode under SVO vector control scheme.*

Key Words: **doubly-fed induction generator (DFIG); stator-voltage-oriented (SVO) vector control; proportional-integral (PI) controller, sub-synchronous resonance (SSR) mode, feed-forward compensation**

1. INTRODUCTION

The most preferred topology for high power (+5 MW) wind applications and currently very popular is Doubly-fed induction generator (DFIG). Its independent active and reactive power control along with variable-speed operation offer many advantages over other fixed-speed topologies [1]. Commercially important advantages of employing DFIG in wind power applications include lower power rating of power electronic interface and ultimately the lower cost. Depending on the orientation of the synchronously rotating dq0 reference frame [2], vector control schemes employed for DFIG are: (1) stator flux orientation (SFO) – d-axis aligned to stator flux vector and (2) stator voltage orientation (SVO) – q-axis aligned to stator voltage vector.

The reactive power production of the DFIG limits the stability [3], when SFO is employed. However, when SVO is employed, such stability problems do not exist [4]. In the analysis of these schemes, it is considered that the rotor current tracks its reference perfectly, ignoring the effect of controller tuning on the stability of DFIG. The dynamics of inner current loop is taken into account in stability analysis of SFO based various implementations of the vector control schemes in [5].

In this paper the inner current loop dynamics are taken into account and the impact of the tuning of PI controllers on the stability of DFIG and SSR mode in SVO is investigated. Pole-assignment technique is followed for controller design. Both the mathematical analysis and simulations reveal that the erroneous tuning of the PI controllers lead to the unstable operation of DFIG and/or can also lead to SSR mode excitation in SVO vector control. The paper is organized as follows: Section II includes the mathematical model of DFIG. The pole-assignment design strategy is detailed in Section III. The state-space model of DFIG system in SVO is presented in Section IV. The stability analysis of DFIG in SVO is carried out in Section V. Simulation evaluation is presented in Section VI and finally the conclusion in Section VII.

2. MATHEMATICAL MODEL OF DFIG SYSTEM

2.1 Park-model of DFIG

The T-equivalent circuit representing the Park Model [6] of DFIG in synchronous reference frame, is shown in Fig.1.

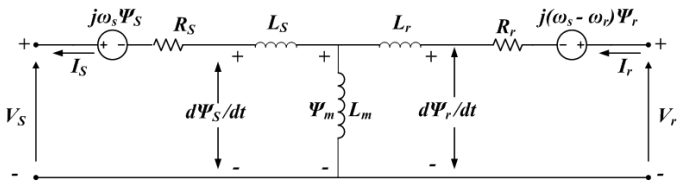

Fig.1 Park Model (T-equivalent circuit) of DFIG in synchronous reference frame

Based on the T-equivalent circuit, the mathematical model of DFIG system in per unit of system base is represented as DFIG equations in synchronously rotating d-q reference frame:

$$v_{qs} = -R_S i_{qs} + \omega_s \psi_{ds} + \frac{1}{\omega_b}\frac{d}{dt}\psi_{qs} \quad (1)$$

$$v_{ds} = -R_S i_{ds} - \omega_s \psi_{qs} + \frac{1}{\omega_b}\frac{d}{dt}\psi_{ds} \quad (2)$$

$$v_{qr} = R_r i_{qr} + (\omega_s - \omega_r)\psi_{dr} + \frac{1}{\omega_b}\frac{d}{dt}\psi_{qr} \quad (3)$$

$$v_{dr} = R_r i_{dr} - (\omega_s - \omega_r)\psi_{qr} + \frac{1}{\omega_b}\frac{d}{dt}\psi_{dr} \quad (4)$$

$$\psi_{qs} = -L_{ss} i_{qs} + L_m i_{qr} \quad (5)$$

$$\psi_{ds} = -L_{ss} i_{ds} + L_m i_{dr} \quad (6)$$

$$\psi_{qr} = L_{rr} i_{qr} - L_m i_{qs} \quad (7)$$

$$\psi_{dr} = L_{rr} i_{dr} - L_m i_{ds} \quad (8)$$

$$L_{ss} = L_s + L_m \quad (9)$$

$$L_{rr} = L_r + L_m \quad (10)$$

where,

$\bar{V}_s = v_{ds} + jv_{qs}$: Stator voltage space vector

$\bar{V}_r = v_{dr} + jv_{qr}$: Rotor voltage space vector referred to stator

$\bar{I}_s = i_{ds} + ji_{qs}$: Stator current space vector

$\bar{I}_r = i_{dr} + ji_{qr}$: Rotor current space vector referred to stator

$\overline{\psi_s} = \psi_{ds} + j\psi_{qs}$: Stator flux-linkage space vector (11)

$\overline{\psi_r} = \psi_{dr} + j\psi_{qr}$: Rotor flux-linkage space vector referred to stator (12)

R_s, R_r : Stator and rotor resistance referred to stator

L_s, L_r : Stator and rotor leakage inductance referred to stator,

L_m: Magnetizing inductance referred to stator,

2.2 RSC Inner Rotor Current Control Loop

Eliminating the stator current and rotor flux linkages from the stator and rotor voltage equations, finally we get the rotor voltage as balance of emfs in the rotor circuit, which is used to derive the rotor current control law.

$$\bar{V}_r = R_r \bar{I}_r + \frac{\sigma L_{rr}}{\omega_b}\frac{d}{dt}\bar{I}_r + \bar{E}_1 + \bar{E}_2 + \bar{E}_3 \quad (13)$$

Thus the rotor voltage equation includes:

The rotor voltage injection: $\bar{V}_R = v_{dr} + jv_{qr}$

A voltage drop across the rotor resistance $R_r\bar{I}_r = R_r(i_{dr} + ji_{qr})$

A cross-coupling induced emf term

$$\bar{E}_1 = -\sigma s_L L_{rr} i_{qr} + j\sigma s_L L_{rr} i_{dr} = E_{d1} + jE_{q1}$$

An induced emf term associated with stator flux

$$\bar{E}_2 = -s_L a_r \psi_{qs} + j s_L a_r \psi_{ds} = E_{d2} + jE_{q2}$$

An induced emf term associated with stator transients

$$\bar{E}_3 = \left(\frac{a_r}{\omega_b}\frac{d}{dt}\psi_{ds}\right) + j\left(\frac{a_r}{\omega_b}\frac{d}{dt}\psi_{qs}\right) = E_{d3} + jE_{q3}$$

An induced emf term in the Thevenin's equivalent inductance (as seen from the rotor with stator short circuited):

$$\frac{\sigma L_{rr}}{\omega_b}\frac{d}{dt}\bar{I}_r = \frac{\sigma L_{rr}}{\omega_b}\frac{d}{dt}(i_{dr} + ji_{qr})$$

Laplace transform of equation (13) and subsequent simplification yields,

$$I_{r(s)} = \frac{V_{r(s)} - [E_{1(s)} + E_{2(s)} + E_{3(s)}]}{\left[s\left(\frac{\sigma L_{rr}}{\omega_b}\right) + R_r\right]} \quad (14)$$

The equation (14) represents the process or plant, how the injected voltage Vr in rotor circuit causes the current Ir. The block diagram of plant is shown in Fig.2. The plant or process can be represented by,

$$G_{p(s)} = \frac{1}{\left[s\left(\frac{\sigma L_{rr}}{\omega_b}\right) + R_r\right]} \quad (15)$$

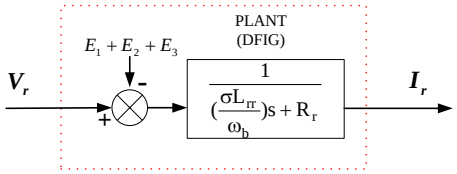

Fig.2 Block diagram of Plant (Open loop system)

The terms E1, E2 and E3 represent the internal disturbances of the plant. From the stator flux-linkage equations (5) & (6), the stator currents can be expressed as:

$$i_{ds} = \frac{-\psi_{ds}}{L_{ss}} + \frac{L_m}{L_{ss}} i_{dr} \quad (16)$$

$$i_{qs} = \frac{-\psi_{qs}}{L_{ss}} + \frac{L_m}{L_{ss}} i_{qr} \quad (17)$$

Substituting these stator currents into stator voltage equations (1) & (2) yields,

$$\frac{d}{dt}\psi_{ds} - \omega_b\omega_s\psi_{qs} + \frac{\omega_b R_s}{L_{ss}}\psi_{ds} = \omega_b\left(v_{ds} - \frac{R_S L_m}{L_{ss}} i_{dr}\right) \quad (18)$$

$$\frac{d}{dt}\psi_{qs} + \omega_b\omega_s\psi_{ds} + \frac{\omega_b R_s}{L_{ss}}\psi_{qs} = \omega_b\left(v_{qs} + \frac{R_S L_m}{L_{ss}} i_{qr}\right) \quad (19)$$

The equations (18) & (19) show that the stator flux and its transients are function of both stator voltage and rotor current, thus the terms E1, E2 and E3 depending on the rotor current and stator flux are the internal disturbances. For compensation of stator flux transient terms, the following equations, derived from equations (18) & (19), are used:

$$\frac{d}{dt}\psi_{ds} = \omega_b\left(v_{ds} + \frac{R_S L_m}{L_{ss}} i_{dr} + \omega_s\psi_{qs} - \frac{R_s}{L_{ss}}\psi_{ds}\right) \quad (20)$$

$$\frac{d}{dt}\psi_{qs} = \omega_b\left(v_{qs} + \frac{R_S L_m}{L_{ss}} i_{qr} - \omega_s\psi_{ds} - \frac{R_s}{L_{ss}}\psi_{qs}\right) \quad (21)$$

For accurate determination of ψ_{ds} and ψ_{qs}, the equations (5) & (6) are used, which require measurement of stator and rotor currents and parameter values of Lss and Lm to be known. Using above equations (20) & (21) the stator flux transients can be accurately determined.

In an SVO, the assumption is usually made that the stator flux is equal in magnitude (for rated stator frequency) to the stator voltage and lags it by 90°. This assumption is valid only under the following conditions:

Semi-steady state condition where the stator flux transients are negligible, i.e $\frac{d}{dt}\overline{\psi_s} = 0$

Negligible stator resistance, i.e Rs = 0.

$$\overline{\psi_s} = -j\frac{\overline{V_s}}{\omega_s} \quad (22)$$

In SVO, $v_{qs} = V_s$ and $v_{ds} = 0$

$$\therefore \psi_{ds} \cong \frac{v_{qs}}{\omega_s} = \frac{V_s}{\omega_s} \quad \text{and} \quad \psi_{qs} \cong -\frac{v_{ds}}{\omega_s} = 0 \quad (23)$$

For exact feed-forward compensation, an observer has to be used based on eq. (5) & (6), i.e the flux is not assumed constant, its variation during the transients is taken into account by considering variations in currents.

The cross-coupling between the d- and q-axis components of the rotor current can be decoupled by using feed-forward compensation.

The generalized control law can be described as,

$\overline{V}_r = \overline{V}'_r$+ Feed-forward Compensation terms (24)

The feed-forward compensation terms simply reflect the internal disturbances:

Cross-coupling term ($\overline{E}_1$)

Stator flux associated induced emf terms ($\overline{E}_2$)

Stator flux transients associated induced emf terms ($\overline{E}_3$)

To provide exact compensation, we need to know the following things accurately:

Machine inductances Lss, Lrr and Lm, which vary over the life period of the machine. So usually estimation of machine inductances is required.

Synchronous speed ωs and rotor speed ωr.

Rotor currents iqr and idr.

Stator flux: Exact determination of stator flux depends on machine inductances and currents. The stator flux $\overline{\psi_s}$ is close to d-axis. Hence, $\psi_{ds} \cong |\psi_s|$ and $\psi_{qs} \cong 0$. Thus for ψ_{ds} we can use exact value or approximate value, but for ψ_{qs}we have to use only exact value.

Accurate or approximate stator flux estimate can be used in compensation. Thus various implementations of the current control law can be described as,

$$\overline{V}_r = \overline{V}'_r + K_1\overline{E}_1 + K_2\overline{E}_2 + \hat{K}_2\hat{\overline{E}}_2 + K_3\overline{E}_3 + \hat{K}_3\hat{\overline{E}}_3 \quad (25)$$

where ^ indicates an approximated quantity.

Various implementations of the feed-forward compensation in inner current loop are summarized in Table I.

Table-1: Implementations of Feed-forward Compensation in inner current loop

Scheme	Feed-forward Compensation Terms	K_1	K_2	$\hat{K}_2$	K_3	$\hat{K}_3$
A	None	0	0	0	0	0
B	Cross-coupling + exact stator flux associated	1	1	0	1	0
C	Cross-coupling + approximate stator flux associated	1	0	1	0	1
D	Only Cross-coupling	1	0	0	0	0
E	Only exact stator flux associated	0	1	0	1	0
F	Only approximate stator flux associated	0	0	1	0	1

The controller output can be described as,

$$\overline{V}'_r = K_p(\bar{I}_{rref} - \bar{I}_r) + K_i\int(\bar{I}_{rref} - \bar{I}_r)dt \quad (26)$$

The generalized closed-loop control strategy is shown in Fig 3.

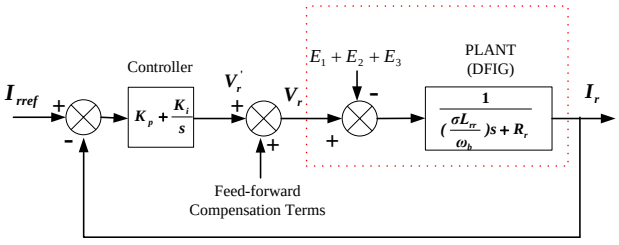

Fig.3 Generalized closed-loop control

If the estimated parameters of compensation terms have the correct values, then from equations (13) and (24) we can write,

$$\bar{V}'_r = R_r\bar{I}_r + \frac{\sigma L_{rr}}{\omega_b}\frac{d}{dt}\bar{I}_r \quad (27)$$

The transfer function between $V'_{r(s)}$ and $I_{r(s)}$ is,

$$G_{(s)} = \frac{I_{r(s)}}{V'_{r(s)}} = \frac{1}{\left[s\left(\frac{\sigma L_{rr}}{\omega_b}\right)+R_r\right]} \quad (28)$$

Assuming that the feed-forward compensation nullifies the effect of disturbances, we have $V'_r = V_r$.

The controller can be designed considering the process model as,

$$G_{p(s)} = \frac{I_{r(s)}}{V'_{r(s)}} = \frac{1}{\left[s\left(\frac{\sigma L_{rr}}{\omega_b}\right)+R_r\right]} = \frac{\left(\frac{\omega_b}{\sigma L_{rr}}\right)}{\left[s+\left(\frac{\omega_b}{\sigma L_{rr}}\right)R_r\right]} \quad (29)$$

2.3 RSC Outer-loop Control Design:

2.3.1 Speed Control Loop:

Speed control of DFIG is essential for MPPT operation. The inner current control loop dynamics is very fast as compared to that of the outer speed control loop. Hence, the effect of inner loop is ignored. The design technique is same as that used for inner current control loop. In SVO, electromagnetic torque is controlled by q-axis rotor current

$$T_e \cong \left(\frac{L_m}{\omega_s L_{ss}}\right) v_{qs} i_{qr} \quad (30)$$

The q-axis rotor current can control speed independently.

Transfer function between speed and q-axis rotor current is given by:

$$\frac{\Omega_{r(s)}}{I_{qr(s)}} \cong \left[\frac{\frac{-L_m V_s}{2H_g\omega_s L_{ss}}}{s+\frac{D_g}{2H_g}}\right] \quad (31)$$

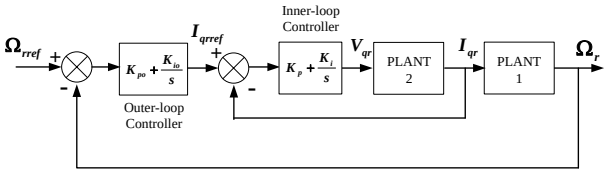

Fig. 4 Speed Control Loop

2.3.2 Reactive Power Control Loop:

Reactive Power control of DFIG is essential for maintaining the power factor. The inner current control loop dynamics is very fast as compared to that of the outer reactive power control loop. Hence, the effect of inner loop is ignored. The design technique is same as that used for inner current control loop.

In SVO, Reactive Power is controlled by d-axis rotor current

$$Q_s = \left(\frac{-V_s\psi_{ds}}{L_{ss}}\right) + \left(\frac{V_s L_m}{L_{ss}}\right) i_{dr} \quad (32)$$

The first term is constant under normal condition and treated as disturbance.

Transfer function between Reactive power and rotor current is given by:

$$\frac{Q_{s(s)}}{I_{dr(s)}} = \left[\frac{V_s L_m}{L_{ss}}\right] \quad (33)$$

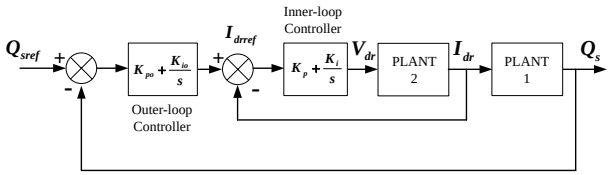

Fig. 5 Reactive Power Control Loop

3. PI-CONTROLLER DESIGN BASED ON POLE-ASSIGNMENT TECHNIQUE

3.1 Pole-assignment design strategy:

The PI controller transfer function is expressed as,

$$C_{(s)} = K_p + \frac{K_i}{s} = K_c\left[1+\frac{1}{\tau_i s}\right] = \frac{K_p s+K_i}{s} \quad (34)$$

The plant transfer function is,

$$G_{p(s)} == \frac{\left(\frac{\omega_b}{\sigma L_{rr}}\right)}{\left[s+\left(\frac{\omega_b}{\sigma L_{rr}}\right)R_r\right]} = \frac{b}{s+a} \quad (35)$$

The closed-loop transfer function T(s) is given by,

$$T_{(s)} = \frac{b(K_p s+K_i)}{s(s+a)+b(K_p s+K_i)} \quad (36)$$

The characteristic equation is,

$$s(s+a)+b(K_p s+K_i) = 0$$

$$s^2+(a+bK_p)s+b(K_i) = 0$$

To determine the controller gains, the characteristic equation is set to its standard form, $s^2+2\zeta\omega_n s+\omega_n^2 = 0$.

The PI controller gains are:

$$K_p = \frac{2\zeta\omega_n - a}{b} \text{ and } K_i = \frac{\omega_n{}^2}{b} \quad (37)$$

3.2 Selection of ζ and ω_n:

Actual system transfer function can be expressed as,

$$T_{(s)} = \frac{b(K_p s+K_i)}{s(s+a)+b(K_p s+K_i)} = \frac{(2\zeta\omega_n - a)s+\omega_n{}^2}{s^2+2\zeta\omega_n s+\omega_n^2} \quad (38)$$

Desired transfer function in standard form,

$$T_{d(s)} = \frac{{\omega_n}^2}{s^2 + 2\zeta\omega_n s + \omega_n^2}$$

With known 'a' and 'b', if attempt is made to select ζ and ωn such that (2ζωn = a) making actual transfer function same as desired one, the proportional gain becomes zero. Therefore, this combination of ζ and ωn is avoided.

Usually the damping coefficient ζ is often chosen as 1 or 0.707 in practice. Therefore, with ζ=0.707, the ωn is so selected that the closed loop poles lie in the left-half of s-plane, leading to system stability. Larger the ωn, wider is the closed-loop bandwidth and faster is the system response. The Bandwidth of the inner current loop dynamics is considered as the tuning parameter for PI controllers.

Here reduced order (first-order) model is used. Actually system is complex (higher-order), so while selecting ωn, its effect on closed-loop dominant poles is considered and that ωn is selected which results in dominant closed-loop poles sufficiently away from the imaginary axis in left-half of s-plane.

It is also useful to choose ωn relative to the bandwidth of the open-loop system $\left[a = \frac{\omega_b R_r}{\sigma L_{rr}}\right]$. Here, a normalized parameter 0<γ<1 is proposed to be used where the desired closed-loop bandwidth is calculated as:

$$\omega_n = \left[\frac{1}{1-\gamma}\right]\frac{\omega_b R_r}{\sigma L_{rr}} \text{ rad/sec} \qquad (39)$$

The parameter γ is often selected around 0.9 to give a satisfactory performance.

4. STATE-SPACE MODEL OF DFIG SYSTEM IN SVO

By eliminating the stator and rotor fluxes in equations (1) to (8), the open-loop state-space model of DFIG is obtained as,

$$\frac{d}{dt}\begin{bmatrix} i_{qs} \\ i_{ds} \\ i_{qr} \\ i_{dr} \end{bmatrix} = A_{OL,1}\begin{bmatrix} i_{qs} \\ i_{ds} \\ i_{qr} \\ i_{dr} \end{bmatrix} + B_{OL,1}\begin{bmatrix} v_{qs} \\ v_{ds} \\ v_{qr} \\ v_{dr} \end{bmatrix} \qquad (40)$$

Referring to equations (24) & (25), taking into account the feed-forward compensation terms of the control law, the open-loop state-space model can be modified to

$$\frac{d}{dt}\begin{bmatrix} i_{qs} \\ i_{ds} \\ i_{qr} \\ i_{dr} \end{bmatrix} = A_{OL,2}\begin{bmatrix} i_{qs} \\ i_{ds} \\ i_{qr} \\ i_{dr} \end{bmatrix} + B_{OL,2}\begin{bmatrix} v_{qs} \\ v_{ds} \\ v'_{qr} \\ v'_{dr} \end{bmatrix} \qquad (41)$$

The state-space model of closed-loop DFIG system is derived by substituting v'_{qr} and v'_{dr} from equation (26) into equation (41) with

$$e_{qr} = -\int (i_{qrref} - i_{qr})\, dt \qquad (42)$$

$$e_{dr} = -\int (i_{drref} - i_{dr})\, dt \qquad (43)$$

$$\frac{d}{dt}\begin{bmatrix} i_{qs} \\ i_{ds} \\ i_{qr} \\ i_{dr} \\ e_{qr} \\ e_{dr} \end{bmatrix} = A_{CL}\begin{bmatrix} i_{qs} \\ i_{ds} \\ i_{qr} \\ i_{dr} \\ e_{qr} \\ e_{dr} \end{bmatrix} + B_{CL}\begin{bmatrix} v_{qs} \\ v_{ds} \\ i_{qrref} \\ i_{drref} \end{bmatrix} \qquad (44)$$

The system has six state variables, hence has six poles, which are obtained from the eigenvalues of the system matrix A_{CL}. For the DFIG parameters mentioned in Table II, the bandwidth is selected and controller gains are computed from equation (37).

For different compensation schemes, the closed-loop poles of the system are determined and found that the system has two very lightly damped poles close to the imaginary axis in s-plane. These are the critical poles that decide the stability of the system.

Table–2: DFIG parameters

Parameter	Value	Parameters	Value
Power Rating	2 MVA	L_s	0.09231 pu
Line Voltage	690 V	L_r	0.09955 pu
Frequency	50 Hz	L_m	3.95279 pu
R_s	0.00488 pu	L_{ss}	4.0451 pu
R_r	0.00549 pu	L_{rr}	4.0523 pu

5. STABILITY ANALYSIS OF DFIG IN SVO

Here the bandwidth (ω_n) of the inner current loop dynamics is considered as the tuning parameter of the PI controllers. In this section, the impact of the bandwidth on the stability and SSR mode of the system is investigated. If the real part of the critical poles becomes positive, the system becomes unstable. The damping ratio (ζ) of the conjugate pair of the critical poles is observed as the measure of the stability. The zero damping ratio or negative value refers to the instability. The eigenvalue analysis is carried out for all feed-forward compensation schemes by varying the speed of DFIG in the range 0.7 pu to 1.2 pu. The observations are as follows:

i) The compensation schemes C and E using approximate stator flux estimate leads to instability.

ii) The scheme D based on only cross-coupling compensation provides better damping as compared to other schemes.

iii) Out of six poles, two poles are critical, they are close to imaginary axis and their damping is less.

iv) For scheme B i.e cross-coupling + exact stator flux associated terms compensation, it is seen that the bandwidth ω_n has no effect on the location of critical poles and also on the damping of stable poles.

6. SIMULATION EVALUATION

6.1 Step Response:

The step responses are plotted for two cases:

i Fixed bandwidth with varying damping ratio

ii Fixed damping ratio with varying bandwidths.

a) By varying ζ with fixed ω_n:

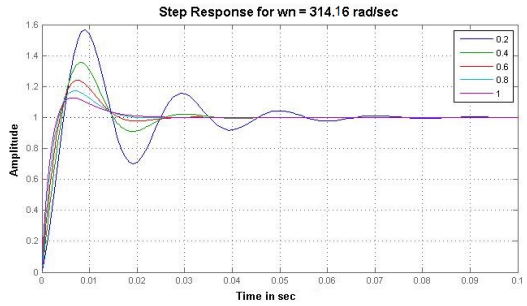

Fig.6 Step-response for ω_n=314.16 rad/sec and ζ varying from 0.2 to 1

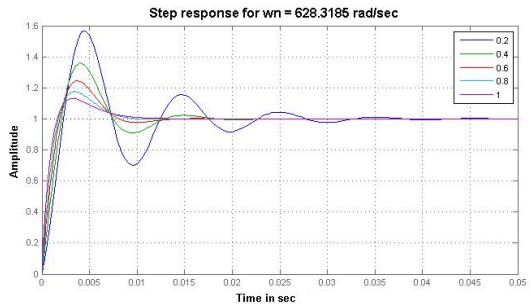

Fig.7 Step-response for ω_n=628.3185 rad/sec and ζ varying from 0.2 to 1

With increase in damping ratio, the peak overshoot and settling time are reduced, as shown in Fig.6 and 7.

For same damping, the settling time reduces with increase in bandwidth. For ζ = 0.2, the settling time reduces from 63.66 millisec to 31.83 millisec when ω_n is doubled.

b) By varying ω_n with fixed ζ :

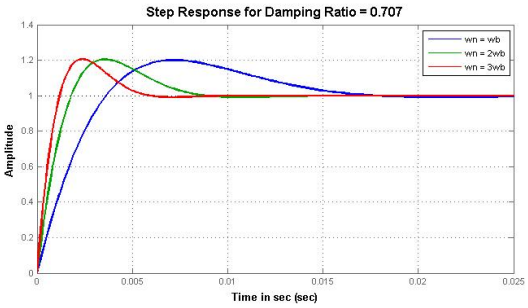

Fig.8 Step-response for ζ = 0.707 and ω_n varying

Referring to Fig. 8, it is seen that overshoot is independent of ω_n. With increase in ω_n, the settling time is reduced

- For ω_n= 314.16 rad/sec, T_s = 18 msec
- For ω_n= 942.48 rad/sec, T_s = 6 msec

The Choice of ω_n is based on :

- Oscillation frequency in synchronous ref. frame
- Susceptibility of system to noise.

6.2 RSC Inner-loop Transient Response:

These plots show the transient response of inner-loop controller for step change in reference values. It is seen that the response is fast.

i) Fig. 9 shows the step response for I_{qrref} = 0.523 pu (constant) and I_{drref} is changed from 0.253 pu to 0.6 pu at t = 1 sec.

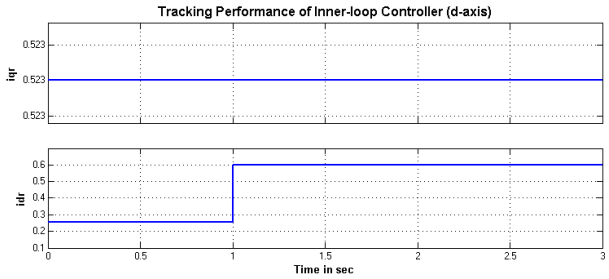

Fig.9 Step-response for I_{qrref} = 0.523 pu (constant) I_{drref} is changed from 0.253 pu to 0.6 pu at t = 1 sec

ii) Fig. 10 shows the step response for I_{drref} = 0.253 pu (constant) and I_{qrref} is changed from 0.75 pu to 1 pu at t = 1 sec.

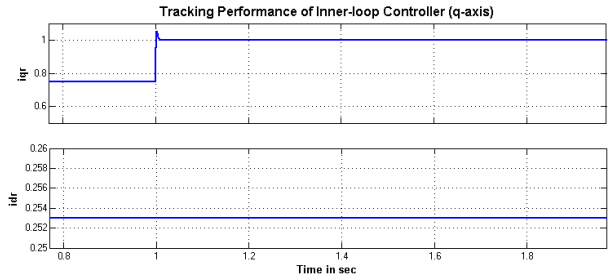

Fig.10 Step-response for I_{drref} = 0.253 pu (constant) I_{qrref} is changed from 0.75 pu to 1 pu at t = 1 sec

6.3 Speed Control Transient Response:

Fig. 11, 12 and 13 show the step response for ζ = 0.707 with varying bandwidth when the reference speed is changed from 1 pu to 1.1 pu at t = 2 sec.

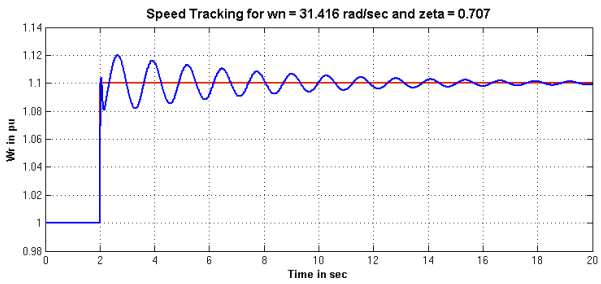

Fig.11 Step-response for ω_n=1.416 rad/sec and ζ=0.707 when Ω_{rref} is changed from 1 pu to 1.1 pu at t = 2 sec

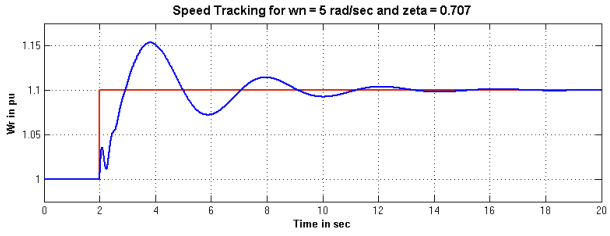

Fig.12 Step-response for ω_n=5 rad/sec and ζ=0.707 when Ω_{rref} is changed from 1 pu to 1.1 pu at t = 2 sec

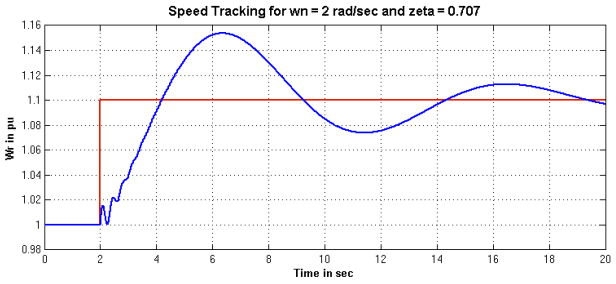

Fig.13 Step-response for ω_n= 2 rad/sec and ζ=0.707 when Ω_{rref} is changed from 1 pu to 1.1 pu at t = 2 sec

These plots show the transient responses for step change in speed reference value for different values of outer-loop bandwidth.
It is seen that –

i) Overshoot increases with decrease in bandwidth.

ii) Oscillation frequency increases with increase in bandwidth

Outer loop bandwidth is selected to be much smaller than that of inner loop.

6.4 Reactive Power Control Transient Response:

Fig. 14, 15 and 16 show the step response for ζ = 0.707 with varying bandwidth when the reference reactive power is changed from 0.5 pu to 0.7 pu at t = 2 sec.

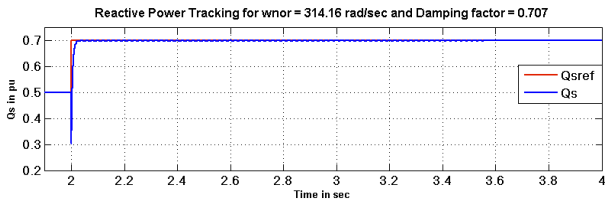

Fig.14 Step-response for ω_n= 314.16 rad/sec and ζ=0.707 when Q_{sref} is changed from 0.5 pu to 0.7 pu at t = 2 sec

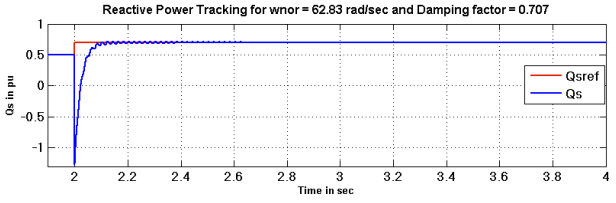

Fig.15 Step-response for ω_n= 62.83 rad/sec and ζ=0.707 when Q_{sref} is changed from 0.5 pu to 0.7 pu at t = 2 sec

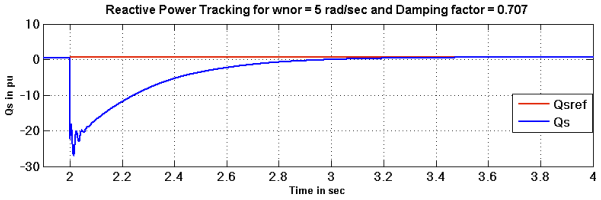

Fig.16 Step-response for ω_n= 5 rad/sec and ζ=0.707 when Q_{sref} is changed from 0.5 pu to 0.7 pu at t = 2 sec

These plots show the transient response for step change in reactive power reference value for different outer-loop bandwidths. For lower bandwidth, much higher negative pulse is observed. Therefore comparatiely higher bandwidth is preferred.

The theoretical analysis is supported through simulations in Matlab/Simulink. Thus the stability is accessed under a small perturbation, which is the change in the reference signal command. The instability of the inner current loop is caused when the bandwidth is wrongly selected which move the critical poles to the unstable region.

7. CONCLUSIONS

i) In SVO, independent control of speed and reactive power is possible using q-axis and d-axis rotor current control respectively employing decoupled control.
ii) For Inner-loop fast current control, higher bandwidth is preferred to avoid the sub-synchronous oscillations and for outer loop comparatively lower bandwidth is chosen.
iii) While selecting bandwidth, the eigenvalue analysis is used to identify the range of bandwidths causing sub-synchronous resonance and oscillations.
iv) The compensation schemes based on approximate stator flux estimation leads to instability.
v) The compensation scheme based on cross-coupling and exact stator flux associated terms is found to be better.

REFERENCES

[1] S. Muller, M. Deicke, R.W. de Doncker: "Doubly fed induction generator systems for wind turbines", IEEE Ind. Appl. Mag., 2002, 8, (3), pp. 26–33

[2] Hopfensperger B., Atkinson D. J., Lakin R. A.: "Stator-flux oriented control of doubly-fed induction machine with and without position encoder", IEE Proc. Electr. Power Appl., 2007, 147, (4), pp. 241-250.

[3] Liu C., Weng H., Sun X., Li F.: "Research of stability of double fed induction motor vector control system", Proc. Int. Conf. Elect. Machines and Systems 2001, 2, (2), pp. 1203-1206.

[4] Petersson A., Harnefors L., Thiringer T.: "Comparison between stator-flux and grid-flux-oriented rotor current control of doubly-fed induction generators", IEEE 35th Annual Power Electronics Specialists Conf. 2004, vol. 1, pp. 482-486.

[5] Petersson A., Harnefors L., Thiringer T.: "Evaluation of current control methods for wind turbines using doubly-fed induction machines", IEEE Trans, Power Electron. 2005,20,(1), pp. 227-235.

[6] S. Chondrogiannis, M. Barnes: "Stability of doubly-fed induction generator under SVO vector control", IET Renewable Power Generation, 2008, Vol. 2, N0. 3, pp. 170-180.

BIOGRAPHIES

1. **Deodatta Y. Shingare**, B.E. (Electrical), M. E. (Electrical Power Systems), is presently persuing Ph. D. at National Institute of Technology, Calicut, Kerla (India). His research area includes DFIG-based wind farm control to provide dynamic support to the grid under contingency conditions.

2. **Dr. Sunil Kumar T. K.**, B.Tech. (Electrical and Electronics Engineering), N.S.S College of Engineering, Palakkad, 1997, M.Tech. (Power System), N.I.T. Jamshedpur , Ph.D. I.I.T Kharagpur, is presently Assistant Professor in the Department of Electrica Engineering, National Institute of Technology, Calicut, Kerla (India). His research area includes Model Matching Controller Design Methods with Applications in Electric Power Systems.